Article

Atomization Characteristics of Special-Design Pneumatic Two-Fluid Nozzles for Helicopter Main Reducers: A Numerical and Experimental Investigation

He Liu, Huiyun Cheng, Yu Dai * **and Xiang Zhu**

College of Mechanical and Electrical Engineering, Central South University, Changsha 410083, China
* Correspondence: 210143@csu.edu.cn

Abstract: Oil mist lubrication can be utilized as an emergency lubrication system in the main reducer of a helicopter. A special-design pneumatic two-fluid nozzle is the crucial system component for atomizing lubricant oil, so exploring the atomization characteristics of the nozzle has a significance on effectively improving oil mist lubrication performance. A CFD (computational fluid dynamics) model with a DPM (discrete phase model) technique and a specialized atomization test system were set up to both numerically and experimentally investigate the nozzle's atomization characteristics. For the atomization properties of the nozzle, the impacts of air pressure, gas–liquid pressure ratio, lubricant oil flow rate, and lubricant oil property factors, including viscosity and surface tension, were investigated. Combining the experimental and the numerical findings reveals that an increasing air pressure and gas–liquid pressure ratio contribute to the atomization effect of the nozzle, especially the air pressure. In addition, a higher lubricant oil flow rate is slightly unfavorable for atomization, but a rise in viscosity and surface tension prevents the atomization of the lubrication oil.

Keywords: atomization characteristics; computational fluid dynamics; discrete phase model; emergency oil mist lubrication; pneumatic two-fluid nozzle

1. Introduction

When the lubrication system of a helicopter main reducer fails and is interrupted, the main reducer will be in a state of oil loss and lack of lubrication, which can easily cause the failure of transmission parts due to gluing, pitting, and deformation [1]. Oil mist lubrication [2] may be utilized as an emergency lubrication system to provide micro-scale and efficient lubrication, maintain a certain lubrication state to the greatest degree possible, and control temperature increase to effectively improve the transmission system's viability. The pneumatic two-fluid nozzle is the essential component for lubricating oil atomization. Its function is to atomize the lubricating oil with high-pressure air to generate tiny droplets, which are then sprayed with compressed air onto the friction surfaces of gears, bearings, etc. for lubrication. Its atomization characteristics directly impact the lubricating efficacy of the oil mist.

Typically, the assessment indices of nozzles' atomization characteristics [3] refer to droplet size, atomization cone angle, droplet range, droplet velocity, droplet size distri-bution, etc. The two main methods utilized to ascertain the atomization properties of pneumatic two-fluid nozzles are experiments and CFD studies. Yoon et al. [4] conducted experimental research on the impact of various air and water injection pressures on the at-omization properties of a two-phase flow nozzle with swirlers. Seyedin et al. [5] employed image processing to analyze the structure and performance of a pressure swirl nozzle by measuring the droplet diameter. According to the outcomes, higher gas pressure improves spray angle while decreasing droplet diameter. Yakut et al. [6] investigated the impact of three distinct nozzle diameters, two distinct nozzle-plate separation lengths, four voltages, and three volumetric flow rates on the electrospray and cooling characteristics. Multiple

tests were undertaken by Sarker et al. [7] to investigate the variations in spray characteristics in different structures and flow rates of air-assisted siphon-type liquid atomizers. Using the technique of high-speed shadowgraphy, Chaudhari et al. [8] investigated the spray properties of fuel at varied injection pressures and ambient gas densities. The outcomes showed that spray breakup is controlled by fuel characteristics, inlet pressure, nozzle structure, and surrounding gas conditions. Gad et al. [9] conducted an experiment to determine the impact of operating conditions and nozzle geometry parameters on the atomization performance of an air-blast nozzle. Using a specifically developed high-pressure spray test setup, Zhang et al. [10] performed an experiment to study the interactions of the air and liquid sprayed from an air-blast nozzle at varying ambient pressures. Sattelmayer et al. [11] utilized a two-dimensional model to examine the atomization performance of the prefilming air-blast nozzle, measured and evaluated the droplet size using light scattering technology, and underlined the importance of air velocity at the atomization edge. Li et al. [12] experimentally and computationally investigated the effect of the flow rate and temperature of liquid and the nozzle pressure on the atomization properties of an externally mixing gas–liquid two-phase nozzle. Han et al. [13] developed and validated a CFD approach for studying the impact of liquid pressure on the atomization properties of an internal mixing air-atomizing nozzle. To simulate diesel spray atomization using a large-eddy simulation (LES) turbulence model, Villiers et al. [14] developed a CFD mode integrated with the volume of fluid (VOF) technique, and Ishimoto et al. [15] improved this method to study and display the three-dimensional configuration of the liquid atomization process through a cylindrical nozzle. Adopting the LES technique, Jones et al. [16] numerically studied the distribution of polydispersed droplets produced by a pressure-swirl atomizer. Using a VOF-to-DPM (volume of fluid to discrete phase model) transition technique and an adaptive mesh refinement (AMR) technique, Nazeer et al. [17] created a CFD approach to investigate the atomization properties of a Y-jet nozzle. Wang et al. [18] created a CFD model to explore the impact of the primary structural factors on the internal flow properties of the pressure atomizer. Based on an LES turbulence model, Yu et al. [19] developed a multiscale CFD method integrated with the VOF technique as well as the AMR approach to explore the atomization properties of the pressure-swirl atomizer. Ludwig et al. [20] built a CFD method to describe pneumatic nozzle liquid atomization and investigated how the simulation parameters affected the speed of the calculated droplets.

The aforementioned research on the atomization characteristics of nozzles is mainly applied in traditional fields, such as agricultural pesticide spraying, coal mine dust removal, engine fuel combustion, etc. However, special-design pneumatic two-fluid nozzles are utilized in the emergency oil mist lubrication systems of helicopter main reducers, which puts higher requirements on them, and there is a lack of research on their atomization characteristics at present. This paper seeks to assess the effect of working conditions on atomization characteristics using CFD simulation and experimental testing. It will provide a theoretical and simulation foundation for research on improving the dry running capacity of helicopter main reducer gears using emergency oil mist lubrication.

2. Methodology

2.1. Governing Equation

The atomization process of pneumatic two-fluid nozzles adheres to the principles of conservation of mass, momentum, and energy:

$$\frac{\partial(\rho V_x)}{\partial x} + \frac{\partial(\rho V_y)}{\partial y} + \frac{\partial(\rho V_z)}{\partial z} + \frac{\partial \rho}{\partial t} = 0 \tag{1}$$

$$
\begin{cases}
\frac{\partial(\rho V_x)}{\partial t} + \frac{\partial(\rho V_x V_x)}{\partial x} + \frac{\partial(\rho V_x V_y)}{\partial y} + \frac{\partial(\rho V_x V_z)}{\partial z} \\
= -\frac{\partial P}{\partial x} + \frac{\partial}{\partial x}\left(\mu \frac{\partial V_x}{\partial x}\right) + \frac{\partial}{\partial y}\left(\mu \frac{\partial V_x}{\partial y}\right) + \frac{\partial}{\partial z}\left(\mu \frac{\partial V_x}{\partial z}\right) + S_{V_x} \\
\frac{\partial(\rho V_y)}{\partial t} + \frac{\partial(\rho V_y V_x)}{\partial x} + \frac{\partial(\rho V_y V_y)}{\partial y} + \frac{\partial(\rho V_y V_z)}{\partial z} \\
= -\frac{\partial P}{\partial y} + \frac{\partial}{\partial x}\left(\mu \frac{\partial V_y}{\partial x}\right) + \frac{\partial}{\partial y}\left(\mu \frac{\partial V_y}{\partial y}\right) + \frac{\partial}{\partial z}\left(\mu \frac{\partial V_y}{\partial z}\right) + S_{V_y} \\
\frac{\partial(\rho V_z)}{\partial t} + \frac{\partial(\rho V_z V_x)}{\partial x} + \frac{\partial(\rho V_z V_y)}{\partial y} + \frac{\partial(\rho V_z V_z)}{\partial z} \\
= -\frac{\partial P}{\partial z} + \frac{\partial}{\partial x}\left(\mu \frac{\partial V_z}{\partial x}\right) + \frac{\partial}{\partial y}\left(\mu \frac{\partial V_z}{\partial y}\right) + \frac{\partial}{\partial Z}\left(\mu \frac{\partial V_z}{\partial z}\right) + S_{V_z}
\end{cases}
\tag{2}
$$

$$
\frac{\partial\left[\rho\left(e + \frac{u^2}{2}\right)\right]}{\partial t} + \nabla \cdot \left[\rho\left(e + \frac{u^2}{2}\right)u\right] = \nabla(pu) + \nabla(k\nabla T) + \rho q + \rho f u
\tag{3}
$$

where ρ denotes the fluid density. V_x, V_y, and V_z represent the velocity vectors along the x, y, and z axes, respectively. μ denotes the fluid viscosity. P represents the pressure acting on the fluid element. S_{Vx}, S_{Vy}, and S_{Vz} connote the generalized source term along the x, y, and z axes, correspondingly. u is the fluid velocity. e denotes the internal energy of a fluid per unit of mass. $u^2/2$ represents the kinetic energy of a fluid per unit of mass. k represents the heat conductivity coefficient, and q denotes the heat distribution function due to radiation or other causes.

2.2. Turbulence Model

As a semi-empirical formula, the standard k-ε turbulence model is insufficiently precise for simulating the large, swirling vortex and streamline curvature of a fluid. On the foundation of the standard k-ε turbulence model, the realizable k-ε turbulence model updated with a new governing equation to increase the turbulence dissipation ratio is more suitable for complex two-fluid, jet flow, and flow separation simulation [21,22].

The realizable k-ε turbulence model [23,24] is a two-equation model; the transport equation for the turbulent kinetic energy k is expressed as:

$$
\frac{\partial(\rho k)}{\partial t} + \frac{\partial(\rho k v_j)}{\partial x_i} = \frac{\partial}{\partial x_i}\left[\left(\mu + \frac{\mu_t}{\sigma_k}\right)\frac{\partial k}{\partial x_j}\right] + G_k + G_b - \rho\varepsilon
\tag{4}
$$

The transport equation for the turbulent dissipation rate ε is described as:

$$
\begin{aligned}
\frac{\partial(\rho\varepsilon)}{\partial t} + \frac{\partial(\rho\varepsilon v_j)}{\partial x_i} = \frac{\partial}{\partial x_i}\left[\left(\mu + \frac{\mu_t}{\sigma_\varepsilon}\right)\frac{\partial\varepsilon}{\partial x_j}\right] + C_{1\varepsilon}\frac{\varepsilon}{k}C_{3\varepsilon}G_b + \\
C_{1\varepsilon}\frac{\varepsilon}{k}G_k - \rho C_{2\varepsilon}\frac{\varepsilon^2}{k}
\end{aligned}
\tag{5}
$$

where μ_t is the turbulent viscosity coefficient and v_j denotes the velocity component. σ_k represents the corresponding Prandtl number of k, its value is 1. σ_ε represents the corresponding Prandtl number of ε, its value is 1.2. G_k is the turbulent kinetic energy generated by the mean velocity gradient. G_b connotes the turbulent kinetic energy generated by buoyancy. $C_{1\varepsilon}$, $C_{2\varepsilon}$, and $C_{3\varepsilon}$ are the empirical constants.

2.3. Discrete Phase-Governing Equations

When the atomizing nozzle is operating, the gas and liquid phases will interact in a complicated and intense manner. The DPM based on the Euler–Lagrange method is always employed to analyze the atomization of liquid and the interaction between droplets in numerical simulations, considering air to be the continuous phase and liquid particles to be the breakable and congregable discrete phase. [25]. The droplet trajectory is tracked in a Lagrangian coordinate system and the distribution of droplets after atomization is determined. The liquid particle volume is very small relative to the whole computational domain, and the volume occupied by the liquid particles can be ignored in space. As a discrete phase, the trajectory of liquid particles is calculated by the action of surface equilibrium, the mass, and quantity transfer of continuous-phase gas. Newton's second

law is used to solve the droplet's velocity and displacement by calculating the force and acceleration of the particle in the Lagrangian coordinate system to figure out its path of motion. This is the equation:

$$\frac{du_p}{dt} = F_D + \frac{g(\rho_p - \rho_g)}{\rho_p} \tag{6}$$

$$F_D = \frac{3}{4} \cdot \frac{C_D \rho_g}{\rho_p d_p{}^2} \cdot |u_g - u_p| \cdot (u_g - u_p) \tag{7}$$

where C_D is the flow-resistant coefficient. F_D is the particle's resistance per unit of mass. u_g and u_p denote the speed of gas and liquid particles, respectively. ρ_g and ρ_p represent the density of gas and liquid particles, respectively. d_p represents the diameter of liquid particles.

2.4. CFD Modeling and Numerical Setup

A special-design pneumatic two-fluid nozzle of interest to the present study was formulated. Specifically, the liquid and gas inlet sizes of the nozzle are 2.5 mm and 2.2 mm, the nozzle exit diameter is 0.8 mm, and the mixing chamber's diameter and length are 3.1 mm and 6.5 mm, respectively. The computational domain consisted of two parts: the internal flow field of the nozzle and the external spray flow field. For efficiency in numerical calculation and atomization characteristics analysis, the external spray flow field was established as a 100 × 100 × 200 mm cuboid. ICEM was exploited for generating tetrahedral meshes of the nozzle's interior fluid domain and hexahedral meshes of the external spray flow field. To reduce calculation time and improve calculation efficiency, the middle part of the axis of the outflow field was locally refined, and the mesh was gradually increased by spreading it out from the middle. Local refinement was also performed for the nozzle's small size and large curvature change. Figure 1 shows the CFD mesh.

(a) **(b)**
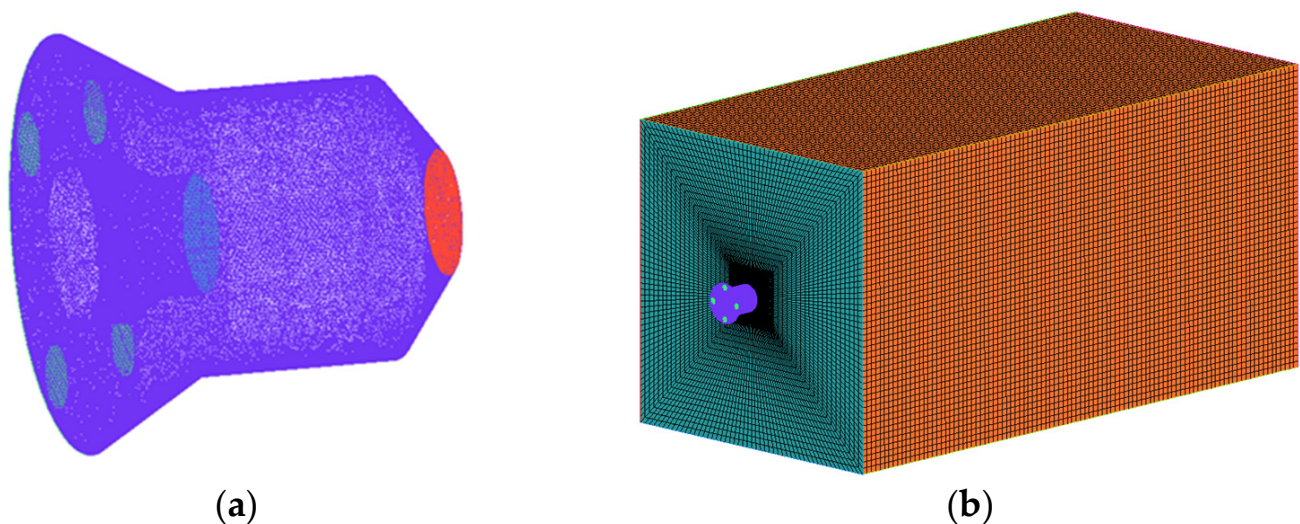
Figure 1. The CFD mesh: (**a**) internal flow field mesh of the nozzle; (**b**) external spray flow field mesh.

ANSYS Fluent 19.2 was utilized to investigate the atomization behavior of the nozzle. The simulation was broken into two parts to optimize efficiency and reduce computing costs. The first part calculated the continuous gas-phase flow field under 3D pressure-based and steady-state solvers and obtained the pressure and velocity information at each point to serve for the next calculation. The second part calculated the coupling flow field of continuous-phase gas and discrete-phase droplets under the transient solver after the first part reached convergence and obtained the atomizing and flow field characteristics of

the pneumatic two-fluid nozzle. The air-blast atomizer, dynamic-drag model, and WAVE breakup model were selected for the discrete phase model.

To guarantee the accuracy of the numerical conclusions, a mesh independence study was conducted by comparing the velocity of gas (VG in m/s) at a 100 mm distance from the nozzle outlet. The change in velocity with the increase in total mesh elements is listed in Table 1. The velocity tended to be stable when the mesh elements increased to Case 3. Therefore, the number of total mesh elements of about 2.08 million was preferred for this paper.

Table 1. Grid independence analysis.

	Number of Grids	V_G
Case 1	206,675	82.86931
Case 2	505,114	88.28088
Case 3	2,082,167	82.12659
Case 4	2,727,160	81.77525
Case 5	3,165,034	81.53322

3. Experiment Test

3.1. Test Rig

To satisfy the clean and environmentally friendly requirement, water was used instead of lubricating oil in this test, and the atomizing gas was air. A photograph of the atomization test system is shown in Figure 2. The test rig was mainly composed of a pneumatic two-fluid nozzle, air compressor, liquid storage tank, pressure gauge, pressure regulating valve, weightometer, an OMEC DP-02 laser particle-size analyzer (test range: 0.5–1500 μm; repeatability error: <3%) and a Phantom VEO-410L high-speed camera. The liquid and gas pressures were adjusted through the pressure regulating valves, the spray images were captured by the camera, and the particle size distribution and average diameter of droplets were measured by the laser particle-size analyzer.
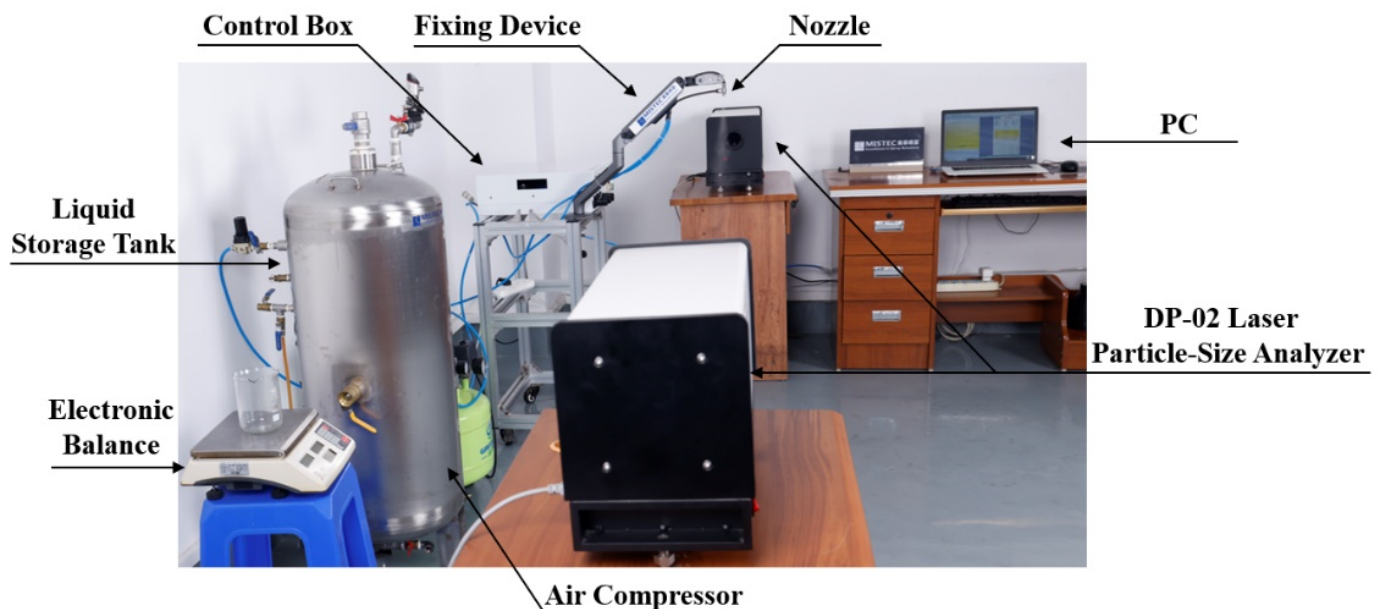
Figure 2. Atomization test system.

The injection system consisted of a pneumatic two-fluid nozzle, pressure hose, and fixed device, shown in Figure 3. The pressurized water entered the nozzle through the pressure hose, mixed with the pressurized air, and formed atomized droplets. The fixing

device was used to support and adjust the nozzle to facilitate the laser particle-size analyzer in measuring the particle size of the droplets on the plane at different distances.

Figure 3. Injection system.

3.2. Verification and Atomization Effect Analysis

Based on the above test rig, the atomization characteristics of the nozzle were tested. Simultaneously, several numerical simulations were conducted under identical conditions. The test and simulation results were compared and analyzed to verify the reliability of the CFD model. In addition, the effects of different gas pressures and gas–liquid pressure ratios on the atomization characteristics were explored through experiments.

3.2.1. Experimental Verification

The nozzle's atomization characteristics were studied using an air pressure (P_a in bar) of 4.0, a water flow rate (F_w in ml/min) of 23, and an outlet pressure of 1 standard atmospheric pressure as examples; the findings are shown in Figure 4. Despite the fact that the real range of atomization was slightly greater owing to the levitation and dissipation of edge droplets during the experiment, the qualitative comparison of the two results is very similar in morphology.

As depicted in Figure 5, the numerical and experimental particle size distribution of the droplets on the plane 120 mm away from the nozzle outlet were investigated. The findings imply that the droplets' size change range laws are very similar. The distribution of the data follows a bell-shaped curve. Furthermore, Figure 6 depicts the SMD of droplets and relative error at different axial distances from the nozzle outlet. Overall, both numerical and experimental results indicate that as distance increases, the SMD tends to slightly rise, and the error between the results is within 15%.
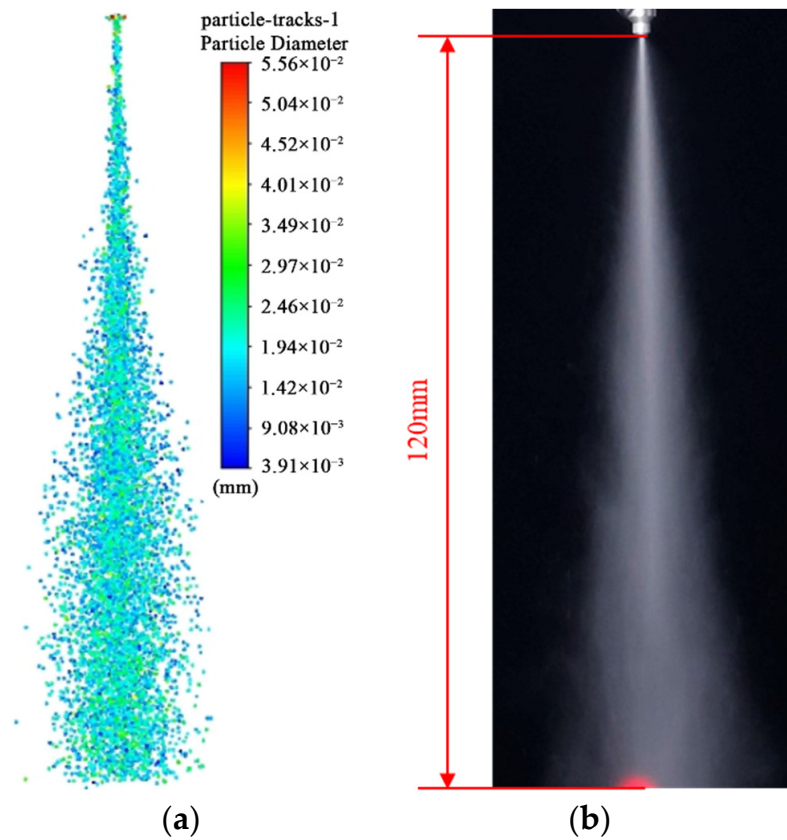
Figure 4. Comparison of atomization jet in the air–water two-phase flow field: (**a**) numerical results; (**b**) experimental findings.
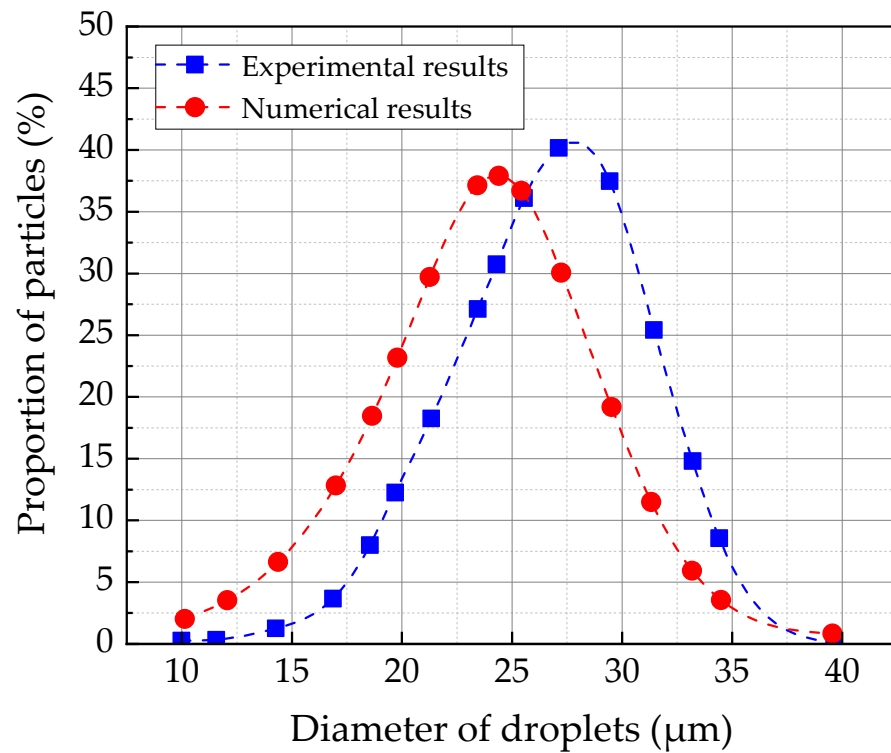

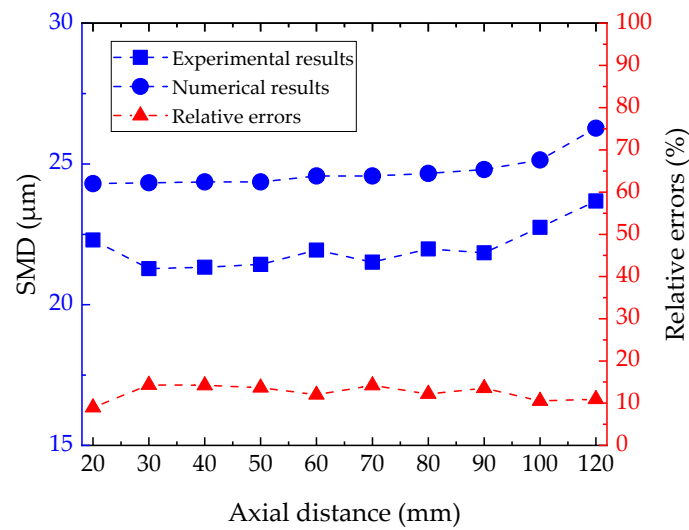**Figure 5.** Comparison of diameter of droplets between numerical results and experimental values.

Figure 6. Droplet size distribution at different axial distances.

To further validate the efficacy of the numerical simulation approach, the F_w was set at 7, 15, and 23, respectively, while all other parameters remained the same. Following the execution of the related tests and numerical studies, a comparison analysis was conducted. Figure 7 shows the experimental and numerical results of atomization features at various water flow rates, indicating that the atomized spray was morphologically similar. As shown in Figure 8, when the water flow rate increased, the SMD increased. Comparing experimental and numerical findings, the error percentage was less than 14%.
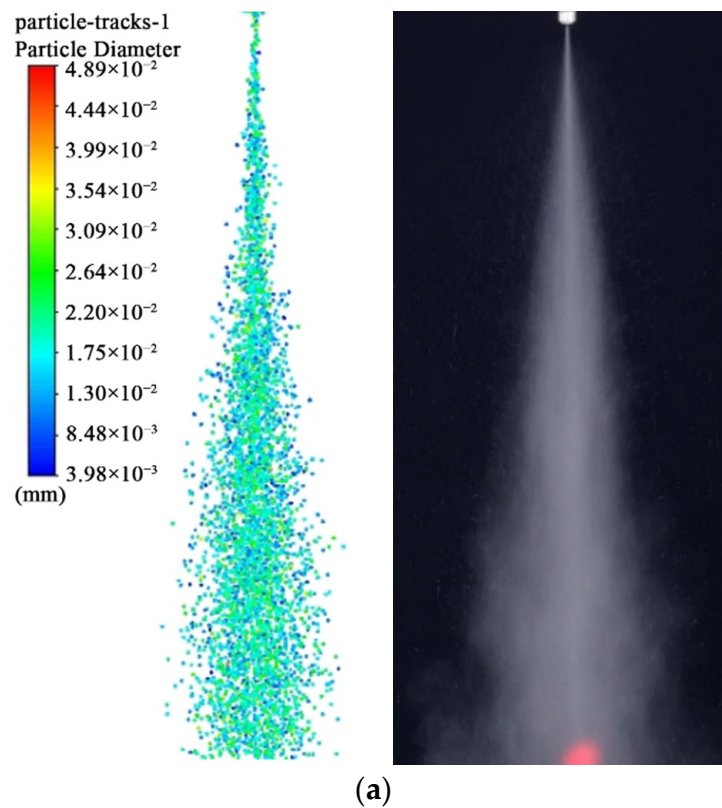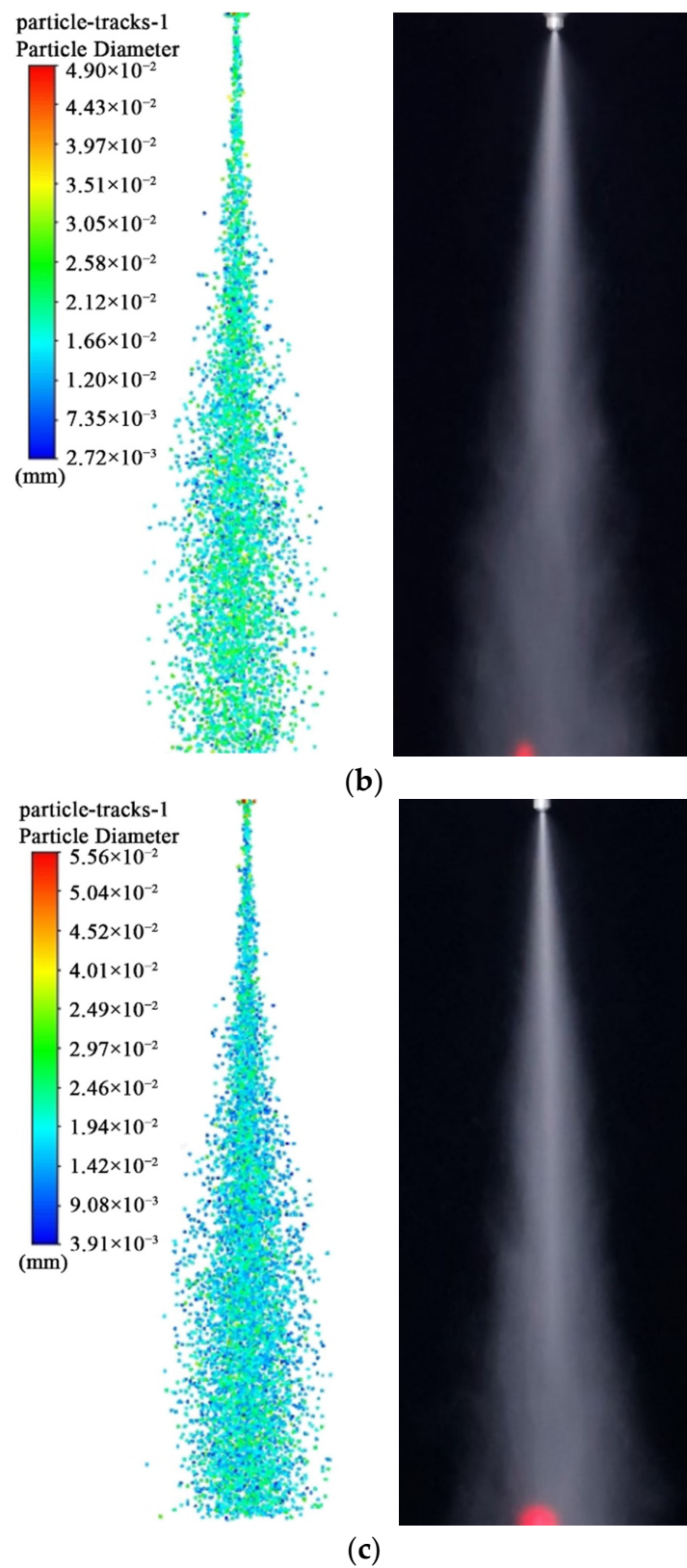

(a)

Figure 7. *Cont.*

(b)

(c)

Figure 7. Comparison of jet atomization with different water flow rates: (**a**) 7 mL/min; (**b**) 15 mL/min; (**c**) 23 mL/min.
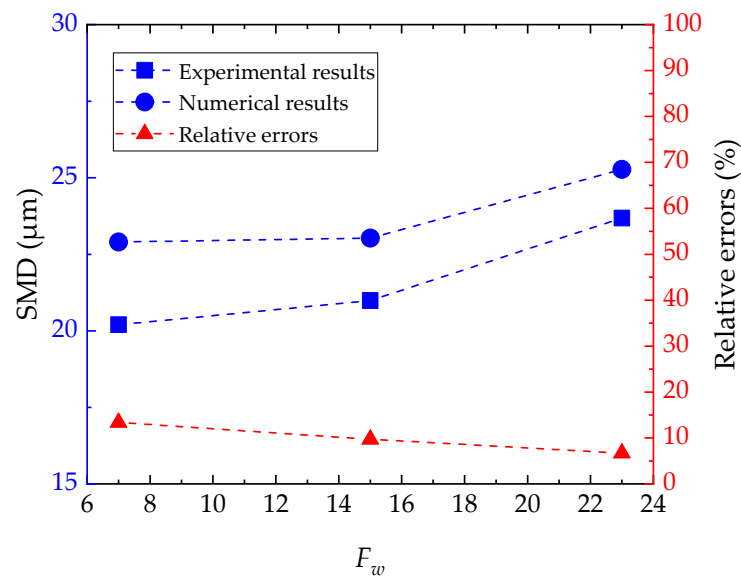
Figure 8. Droplet size distribution at different water flow rates.

Overall, comparison of the qualitative and quantitative aspects of the experimental and simulation findings reveals that the change trends were consistent, and the error is less than 15%, confirming the accuracy and reliability of the numerical method used in this paper.

3.2.2. Effect of Air Pressure

The effects of air pressures on atomization characteristics were also explored through experiments, with the water pressure (P_w in bar) set at 3.0 and the P_a set at 3.0, 3.5, 4.5, and 5.0, respectively. Figure 9 depicts the properties of the atomizing distribution at different air pressures. The spray cone angle is seen to grow larger as air pressure is raised, mainly because the increased air pressure makes the water atomization more thorough and forms more uniform micro-diameter droplets that suspend and float in the air. Figure 10 demonstrates that as the gas pressure goes up, the SMD goes down, while the decreasing trend gradually slows down.
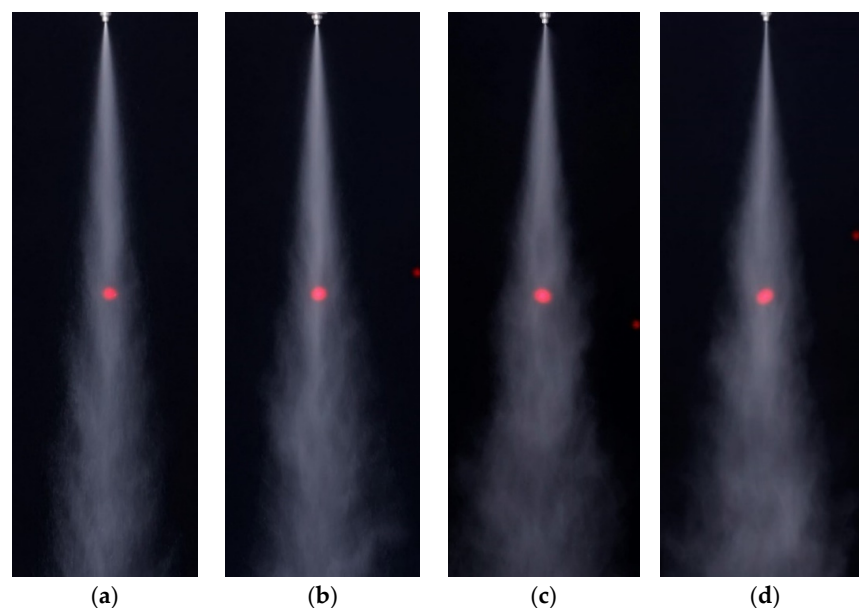

Figure 9. Jet atomization with different air pressures: (**a**) 3.0 bar; (**b**) 3.5 bar; (**c**) 4.5 bar; (**d**) 5.0 bar.
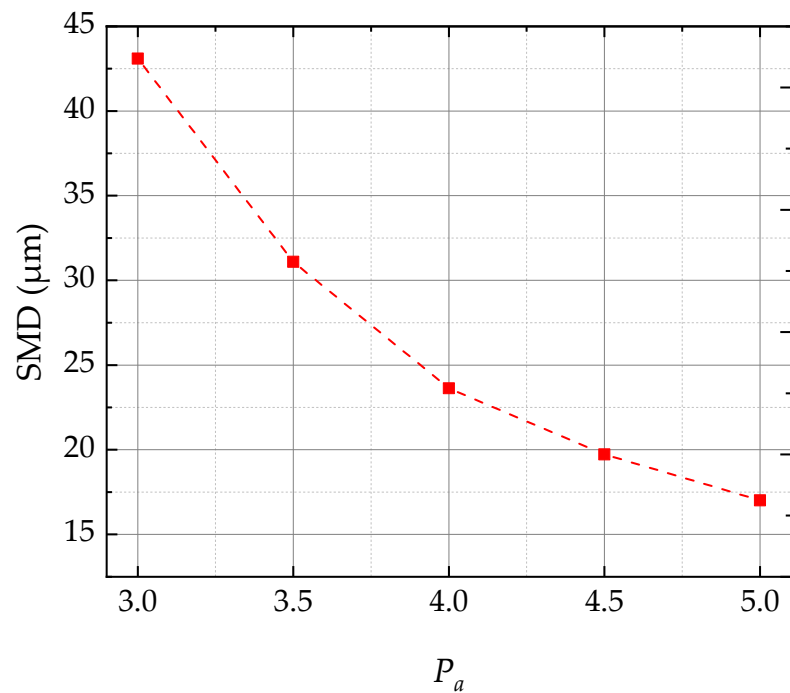
Figure 10. Droplet size distribution at different air pressures.

3.2.3. Effect of Gas–Liquid Pressure Ratio

The gas–liquid pressure ratio (R_{GL}) is also a very important factor affecting atomization characteristics, so the atomization performance of the nozzle under different pressure ratios was investigated through experiments. Figure 11 illustrates the properties of atomization dispersion under varied gas–liquid pressure ratios. As the pressure ratio rose, the atomization performance became more prominent. The larger the gas–liquid pressure ratio was, the greater the aerodynamic force of the air was, the better the atomization effect was, and the greater the area where the uniform micro-diameter droplets suspended and floated.
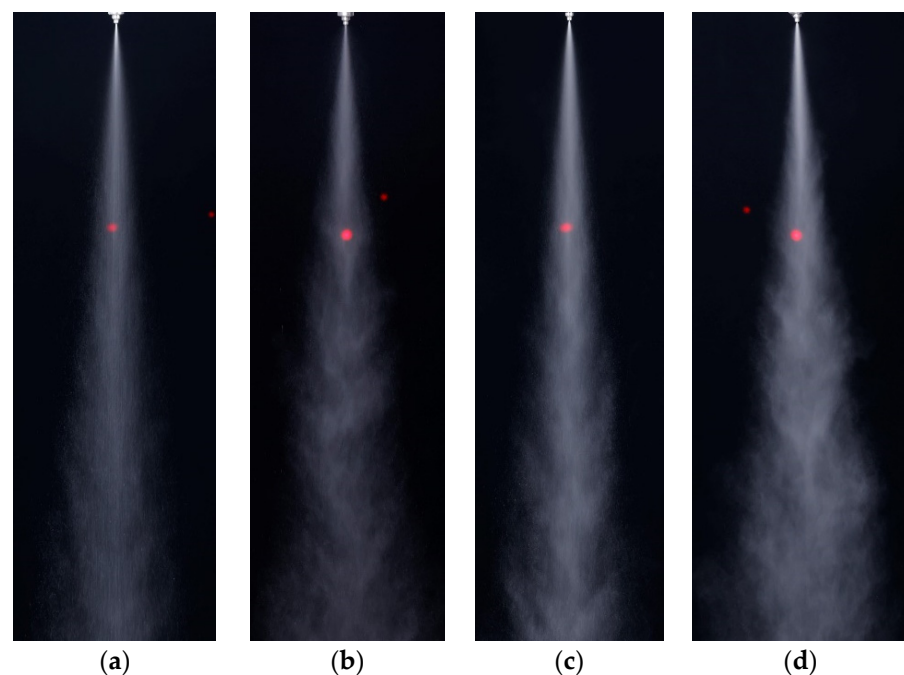

Figure 11. Jet atomization with different gas–liquid pressure ratios: (**a**) 0.89; (**b**) 1; (**c**) 1.25; (**d**) 1.39.

As illustrated in Figure 12 and Table 2, the SMD of droplets decreased when the gas–liquid pressure ratio rose, indicating that the increasing pressure ratio contributed to the nozzle's atomizing action. Furthermore, a rise in air pressure decreased the SMD, whereas an increase in water pressure increased the SMD. When the ratio of gas–liquid pressure equaled 1, the SMD of droplets was 39.95 µm at 4.0 bar and 43.17 µm at 3.0 bar. These suggest that the gas–liquid pressure ratio is a notable factor for atomization, especially the aspect of air pressure.
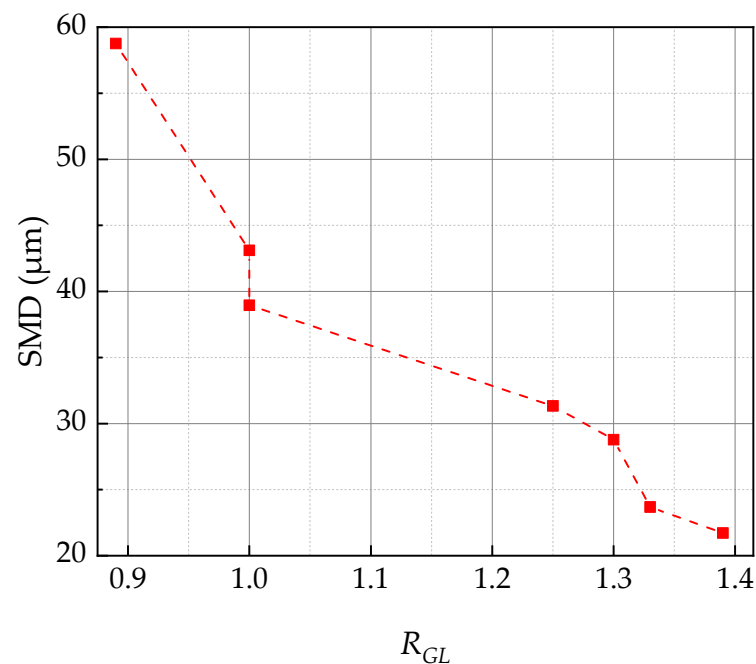

Figure 12. Droplet size distribution at different gas–liquid pressure ratios.

Table 2. SMD at different gas–liquid pressure ratios.

| P_a	P_w	R_{GL}	SMD
5.0	3.6	1.39	21.71
4.0	3.0	1.33	23.68
3.0	2.3	1.30	28.77
2.5	2.0	1.25	31.33
3.0	3.0	1	43.17
4.0	4.0	1	38.95
4.0	4.5	0.89	58.75

4. Numerical Results

In emergency oil-mist lubrication of a helicopter main reducer, the atomization characteristics of the pneumatic two-fluid nozzle have a significant impact on lubricating performance. Through experimental studies, the reliability of the simulation approach and the significance of gas pressure were confirmed. In the following simulation studies, the liquid employed was aviation lubricating oil, and the atomizing gas was air. The impacts of air pressure, lubricant oil flow rate, and lubricant oil property parameters such as viscosity and surface tension on the nozzle's atomization characteristics were investigated using the diameter distribution and SMD of droplets as assessment indices. To acquire spray information data during the CFD simulation, a monitoring surface 150 mm from the nozzle outlet was established in Fluent.

4.1. Effect of Air Pressure

The effects of air pressures on atomization characteristics were explored when the lubricant oil flow rate (F_o in kg/s) was 0.0005, viscosity (v_o in kg/m·s) was 0.0247, and surface tension (σ_o in N/m) was 0.03. The P_a was set at 1.2, 1.5, 2.0, 2.5, 3.0, and 3.5, respectively.

Figure 13a shows the diameter distribution of droplets in 20 μm intervals obtained through the monitoring surface at various inlet air pressures, and Figure 13b presents the corresponding SMD of droplets. As air pressure rose, the distribution range of droplet sizes decreased, and the proportion of small-diameter droplets increased gradually. When the air pressure was 3.5 bar, the proportion of droplets with particle sizes ranging from 0 to 20 μm exceeded 90%, and the atomization effect was superior to all other cases. The SMD of droplets decreased from 74.46 μm at 1.2 bar to 26.46 μm at 3.5 bar. It can be deduced from this that the increase in air pressure has a beneficial impact on the atomization effect. This is mostly because when inlet air pressure increases, gas flow and velocity increase, as does the initial kinetic energy of the gas. Therefore, there will be more energy needed to overcome the lubricant oil's surface tension, viscosity force, and other resistances to achieve atomization. However, the slope of the curve tends to be flat, indicating that it is reaching the limit of the atomization effect of this type of nozzle. This confirms the model's reliability once again, as it demonstrates the same tendency as an experiment in which water was used. The promotion effect of increasing air pressure on atomization gradually weakens. A further increase in air pressure will increase energy consumption, which is unfavorable for economy.
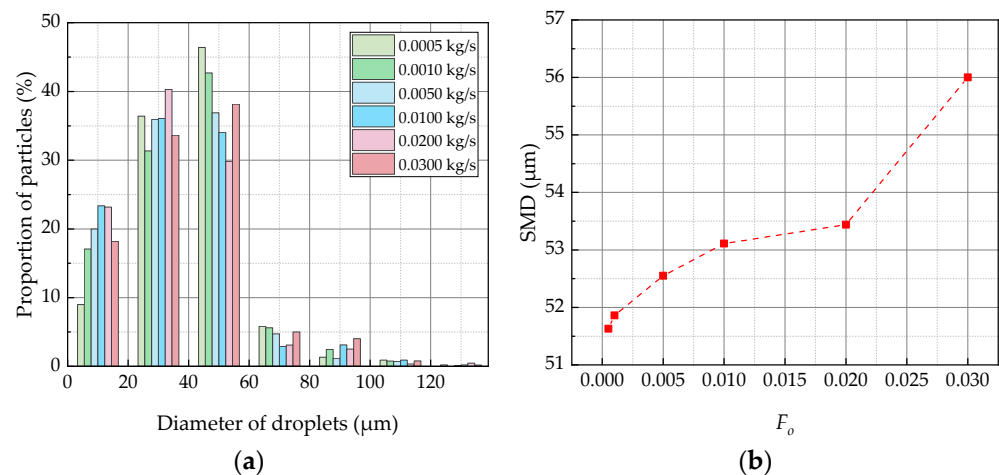

(a)　　　　　　　　　　　　　　　　　　　　(b)
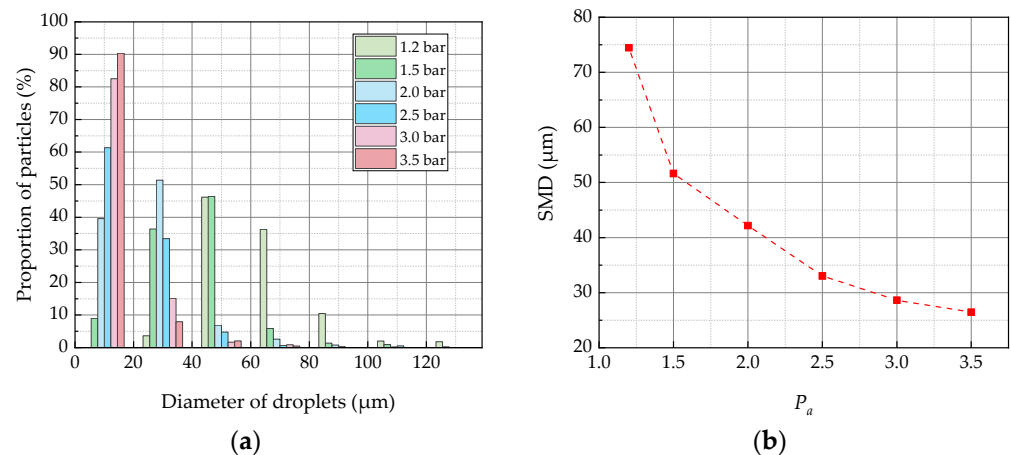
Figure 13. Atomization characteristics of the nozzle at various air pressures: (**a**) diameter distribution of droplets; (**b**) SMD of droplets.

4.2. Effect of Oil Flow Rate

In the subsequent simulation cases, the influence of oil flow rate on atomization characteristics was investigated with the P_a set at 1.5, the v_o at 0.0247, and the σ_o at 0.03. The F_o was set at 0.0005, 0.001, 0.005, 0.01, 0.02, and 0.03, respectively.

Figure 14a demonstrates that at varied lubricant oil flow rates, the diameter distribution of droplets is similar, with particle sizes ranging from 20 to 60 μm being the majority. In Figure 14b the SMD of droplets slightly increased from 51.63 μm when the lubricant oil flow rate was 0.0005 kg/s to 56.17 μm when the lubricant oil flow rate was 0.03 kg/s. It can be concluded that increasing the flow of lubricating oil is marginally detrimental to the atomization effect. That is, with a rise in lubricating oil flow rate, more energy is needed to overcome the lubricant oil's surface tension, viscosity force, and other resistances to achieve atomization. However, as the inlet air setting remains unchanged, the lubricating oil flow rate increases result in a decrease in atomization performance.
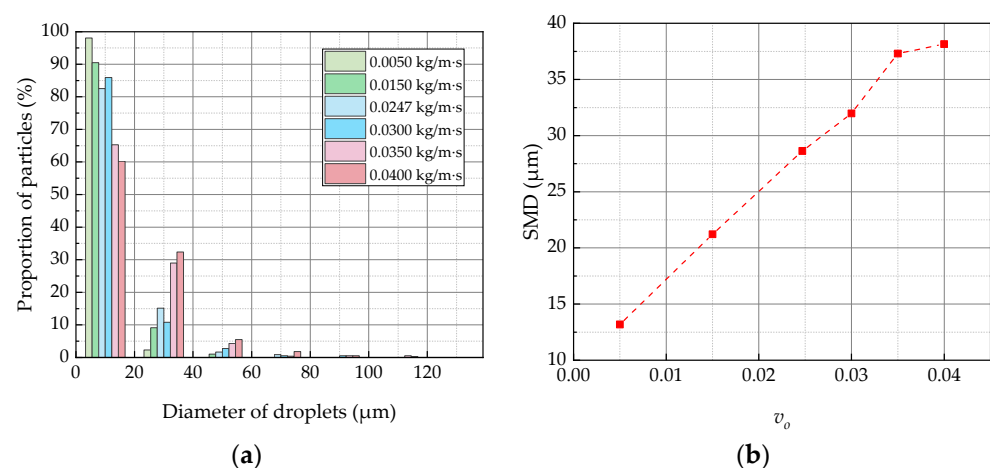
Figure 14. Atomization characteristics of the nozzle at various oil flow rates: (**a**) diameter distribution of droplets; (**b**) SMD of droplets.

4.3. Effect of Oil Viscosity

In the simulation cases below, the effects of oil viscosity on atomization characteristics were studied with the P_a set at 3.0, the F_o at 0.0005, and the σ_o at 0.03. The v_o was set at 0.005, 0.015, 0.0247, 0.03, 0.035, and 0.04, respectively.

Figure 15a demonstrates that the droplet size was predominantly dispersed between 0 μm and 40 μm. Low-viscosity lubricant oil had a higher proportion of droplets in the 0 μm to 20 μm size range; for a lubricating oil viscosity of 0.005 kg/m·s this accounted for 98% of droplets. The proportion for high-viscosity lubricant oil droplets is higher in the 20 to 40 size range; the proportion for lubricant oil with a viscosity of 0.005 kg/m·s was 32%. Figure 15b shows that the SMD of droplets increased from 13.18 μm to 38.15 μm as the viscosity of lubricant oil rose from 0.005 kg/m to 0.04 kg/m, indicating that the higher viscosity of a lubricant oil reduces the atomization effect. That is, the viscosity is the embodiment of the internal friction resistance of lubricant oil. The greater the viscosity, the more the viscosity resistance needs to be overcome when the lubricant oil is atomized. With other settings unchanged, the diameter of atomized lubricant oil droplets will increase accordingly.
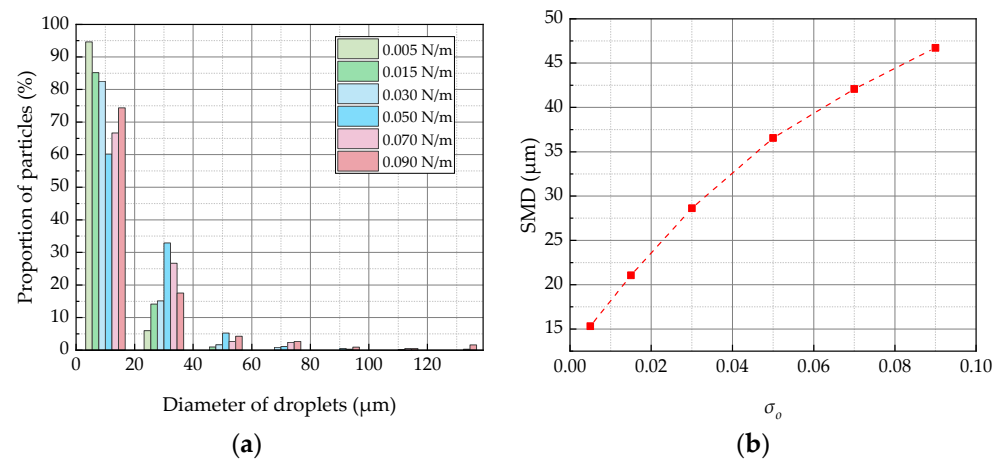

Figure 15. Atomization characteristics of the nozzle for various oil viscosities: (**a**) diameter distribution of droplets; (**b**) SMD of droplets.

4.4. Effect of Oil Surface Tension

In the following simulation cases, the effects of oil surface tension on atomization characteristics were examined with the P_a set at 3.0, the F_o at 0.0005, and the v_o at 0.0247. The σ_o was set at 0.005, 0.015, 0.03, 0.05, 0.07, and 0.09, respectively.

Figure 16a depicts that the primary distribution range of droplet sizes was from 0 μm to 40 μm. Lubricant oil with lower surface tension had a higher proportion of droplets in the 0 μm to 20 μm size range. When the surface tension of the lubricant oil was 0.005 N/m, this range accounted for 94% of droplets. Lubricant oil with high surface tension had a higher percentage of droplets in the size range of 20 μm to 40 μm; when the surface tension was 0.05 N/m, they accounted for 33% of droplets. In addition, with an increase in surface tension, the distribution range of droplet size increased. When the surface tension was 0.09 N/m, the maximum droplet size exceeded 120 μm. The SMD of droplets increased from 15.31 μm to 46.72 μm as the surface tension rose from 0.005 N/m to 0.09 N/m, as shown in Figure 16b. Thus, an increase in lubricant oil surface tension diminishes the atomization effect. This is because surface tension is the force that prevents the lubricating oil from losing its original shape. Consequently, as the surface tension of the lubricant oil increases, so does the resistance that must be overcome during atomization. Keeping all other parameters unchanged, the diameter of lubricating atomized oil droplets will grow correspondingly.

Figure 16. Atomization characteristics of the nozzle at various oil surface tensions: (**a**) diameter distribution of droplets; (**b**) SMD of droplets.

5. Conclusions

This study takes the special-design pneumatic two-fluid nozzle of the emergency oil mist lubrication system of a helicopter main reducer as the research object and analyzes the influence of different working conditions on the atomization characteristics of the nozzle. A CFD model with the DPM approach and a specialized atomization test system were established to computationally and experimentally explore the pneumatic two-fluid nozzle's atomization characteristics. For the atomization properties of the nozzle, the effects of air pressure, gas–liquid pressure ratio, lubricant oil flow rate, and lubricant oil property parameters including viscosity and surface tension were explored. The experimental outcomes were effectively simulated numerically, and a fine correlation was observed between the experimental and simulation outcomes. The main conclusions are as follows:

Firstly, higher air pressure shows a positive impact on the nozzle's atomization action; however, if the inlet pressure rises further, reaching the atomization capacity limit of this type of nozzle, this effect will weaken.

Secondly, the gas–liquid pressure ratio is an important factor for atomization. An increasing gas–liquid pressure ratio contributes to the atomization characteristics of the nozzle, especially the aspect of air pressure.

Thirdly, a rise in the lubricant oil flow rate led to a slight increment in the SMD of the droplets, which is unfavorable to the atomization effect of the nozzle.

Finally, a major element inhibiting lubricating oil from atomizing is a rise in viscosity and surface tension.

In the future, research will be carried out studying a changed nozzle structure to obtain more universal influence rules. Furthermore, corresponding gear and bearing models can be established in the external flow field of the nozzle to study the oil film thickness formed by spray droplets on the surface of the gear and bearing as well as the temperature change of the gear and bearing.

Author Contributions: Conceptualization, H.L. and Y.D.; data curation, H.C. and X.Z.; formal analysis, Y.D.; funding acquisition, H.C.; investigation, X.Z.; methodology, H.L.; project administration, Y.D.; resources, H.C.; software, H.L.; supervision, Y.D. and X.Z.; validation, Y.D., H.C., and X.Z.; visualization, X.Z.; writing—original draft, H.L.; writing—review and editing, H.C. All authors have read and agreed to the published version of the manuscript.

Institutional Review Board Statement: Not applicable.

Informed Consent Statement: Not applicable.

Data Availability Statement: All data are contained within the article.

Conflicts of Interest: The authors declare no conflict of interest.

References

1. Faruck, A.A.M.; Hsu, C.-J.; Doerr, N.; Weigand, M.; Gachot, C. How lubricant formulations and properties influence the performance of rotorcraft transmissions under loss of lubrication conditions. *Tribol. Int.* **2020**, *151*, 106390. [CrossRef]
2. Tawakoli, T.; Hadad, M.; Sadeghi, M. Influence of oil mist parameters on minimum quantity lubrication—MQL grinding process. *Int. J. Mach. Tools Manuf.* **2010**, *50*, 521–531. [CrossRef]
3. Murugan, R.; Balusamy, S.; Kolhe, P. Experimental Study of Liquid Spray Mode of Twin Fluid Atomizer Using Optical Diagnostic Tool. *Flow Turbul. Combust.* **2021**, *106*, 261–289. [CrossRef]
4. Yoon, S.H.; Kim, D.Y.; Kim, D.K.; Kim, B.H. Effect of nozzle geometry for swirl type twin-fluid water mist nozzle on the spray characteristic. *J. Mech. Sci. Technol.* **2011**, *25*, 1761–1766. [CrossRef]
5. Seyedin, S.H.; Ahmadi, M.; Seyedin, S.V. Design and construction of the pressure swirl nozzle and experimental investigation of spray characteristics. *Teh. Glas.* **2019**, *13*, 204–212. [CrossRef]
6. Yakut, R.; Yakut, K.; Sabolsky, E.; Kuhlman, J. Experimental determination of cooling and spray characteristics of the water electrospray. *Int. Commun. Heat Mass Transf.* **2021**, *120*, 105046. [CrossRef]
7. Sarker, M.; Rahman, M.S.; Mandal, S.; Rony, M. A Study on Aerosol Spray Characteristics of Different Size Atomizers. *Aerosol Sci. Eng.* **2020**, *4*, 306–319. [CrossRef]
8. Chaudhari, V.; Kulkarni, A.; Deshmukh, D. Spray characteristics of biofuels for advance combustion engines. *Clean. Eng. Technol.* **2021**, *5*, 100265. [CrossRef]
9. Gad, H.; Ibrahim, I.; Abdel-Baky, M.; Abd El-samed, A.; Farag, T. Experimental study of diesel fuel atomization performance of air blast atomizer. *Exp. Therm. Fluid Sci.* **2018**, *99*, 211–218. [CrossRef]
10. Zhang, Z.; Liu, Y.; Hu, H. Effects of chamber pressure on the kinematic characteristics of spray flows exhausted from an airblast atomizer. *Exp. Therm. Fluid Sci.* **2022**, *130*, 110514. [CrossRef]
11. Sattelmayer, T.; Wittig, S. Internal flow effects in prefilming airblast atomizers Mechanisms of atomization and droplet spectra. *ASME J. Eng. Gas Turbines Power* **1986**, *108*, 465–472. [CrossRef]
12. Lilan, H.; Qian, J.; Pan, N. Study on atomization particle size characteristics of two-phase flow nozzle. *J. Intell. Fuzzy Syst.* **2021**, *40*, 7837–7847. [CrossRef]
13. Han, H.; Wang, P.; Li, Y.; Liu, R.; Tian, C. Effect of water supply pressure on atomization characteristics and dust-reduction efficiency of internal mixing air atomizing nozzle. *Adv. Powder Technol.* **2020**, *31*, 252–268. [CrossRef]
14. Villiers, E.D.; Gosman, D.; Weller, H. Detailed Investigation of Diesel Spray Atomization Using Quasi-Direct CFD Simulation(Spray Technologies, Atomization). *Int. Symp. Diagn. Model. Combust. Intern. Combust. Engines* **2004**, *2004*, 295–302. [CrossRef]
15. Ishimoto, J.; Hoshina, H.; Tsuchiyama, T.; Watanabe, H.; Haga, A.; Sato, F. Integrated simulation of the atomization process of a liquid jet through a cylindrical nozzle. *Interdiscip. Inf. Sci.* **2007**, *13*, 7–16. [CrossRef]
16. Jones, W.P.; Marquis, A.J.; Noh, D. An investigation of a turbulent spray flame using Large Eddy Simulation with a stochastic breakup model. *Combust. Flame* **2017**, *186*, 277–298. [CrossRef]

17. Nazeer, Y.; Ehmann, M.; Sami, M.; Gavaises, M. Atomization mechanism of internally mixing twin-fluid y-jet atomizer. *J. Energy Eng.* **2021**, *147*, 04020075. [CrossRef]

18. Wang, J.; Xu, C.; Zhang, Y.; Zhou, G. Numerical study of the effect of geometric parameters on the internal flow of a pressure nozzle for dustfall. *Adv. Powder Technol.* **2021**, *32*, 1561–1572. [CrossRef]

19. Yu, H.; Jin, Y.-C.; Cheng, W.; Yang, X.; Peng, X.; Xie, Y. Multiscale simulation of atomization process and droplet particles diffusion of pressure-swirl nozzle. *Powder Technol.* **2021**, *379*, 127–143. [CrossRef]

20. Ludwig, W.; Zając, D.; Ligus, G.; Korman, P. Analysis of pneumatic nozzle operation with the stochastic Euler-Lagrange model. *Chem. Eng. Sci.* **2019**, *197*, 386–403. [CrossRef]

21. Bazdidi-Tehrani, F.; Zeinivand, H. Presumed PDF modeling of reactive two-phase flow in a three-dimensional jet-stabilized model combustor. *Energy Convers. Manag.* **2010**, *51*, 225–234. [CrossRef]

22. Huang, L.; Kumar, K.; Mujumdar, A. Simulation of a spray dryer fitted with a rotary disk atomizer using a three-dimensional computional fluid dynamic model. *Dry. Technol.* **2004**, *22*, 1489–1515. [CrossRef]

23. Shih, T.-H.; Liou, W.W.; Shabbir, A.; Yang, Z.; Zhu, J. A new k-ϵ eddy viscosity model for high reynolds number turbulent flows. *Comput. Fluids* **1995**, *24*, 227–238. [CrossRef]

24. Sun, H.; Yan, P.; Tian, L.; Ren, G.; Xu, Y.; Sheng, Z. Effects of Hydrogen Multijet and Flow Rate Assignment on the Combustion Flow Characteristics in a Jet-Stabilized Combustor. *ACS Omega* **2021**, *6*, 12952–12964. [CrossRef] [PubMed]

25. Zahari, N.M.; Zawawi, M.H.; Sidek, L.M.; Mohamad, D.; Itam, Z.; Ramli, M.Z.; Syamsir, A.; Abas, A.; Rashid, M. Introduction of discrete phase model (DPM) in fluid flow: A review. *AIP Conf. Proc.* **2018**, *2030*, 020234. [CrossRef]